Evaluating the Impact of Back Diffusion on Groundwater Cleanup Time

Robert C. Borden[a] and Ki Young Cha[b]

Submitted to

Journal of Contaminant Hydrology

August 2021

[a] North Carolina State University, Campus Box 7908, Raleigh, NC, 27695, USA

rcborden@ncsu.edu

[b] Draper Aden Associates, 114 Edinburgh South Drive, Cary, NC 27511, USA;

kiyoung.cha@gmail.com

Corresponding Author:

Robert C Borden, PhD, PE

Department of Civil, Construction and Environmental Engineering

North Carolina State University

Current Mailing Address: 5017 Theys Rd, Raleigh, NC 27606 USA

Mobile Phone: 919-349-8472

Emails: rcborden@ncsu.edu

Abstract

Back diffusion of groundwater contaminants from low permeability (K) zones can be a major factor controlling the time to reach cleanup goals in downgradient monitor wells. We identify the aquifer and contaminant characteristics that have the greatest influence on the time (T_{OoM}) after complete source removal for contaminant concentrations to decline by 1, 2 and 3 Orders-of-Magnitude (T_1, T_2 and T_3). Two aquifer configurations are evaluated: (a) layered geometry (LG) with finite thickness low K layers; and (b) boundary geometry (BG) with thick semi-infinite low K boundaries. A semi-analytical modeling approach (Muskus and Falta, 2018) is used to simulate the concentration decline following source removal for a range of conditions and generate ≈21,000 independent values of T_1, T_2 and T_3. Linear regression is applied to interpret this large dataset and develop simple relationships to estimate T_{OoM} from three characteristic parameters – the mass residence time (T_M), diffusion time (T_D), and ratio of low K to high K mass storage (γ). T_M is most important predictor of T_1, T_2 and T_3 for both geometries and is equal to the combined high and low K contaminant mass divided by the mass flux, at the end of the loading period (T_L). For LG, T_3 is strongly influenced by $T_D = R_L L_D^2/(4D^*)$, where R_L is the low K retardation factor, L_D is the half-thickness of the embedded low K layers, and D^* is the effective diffusion coefficient. For BG, T_3 is strongly influenced by γ. Contaminant decay in low K zones can significantly reduce cleanup times when $\lambda_L T_D > 0.01$, where λ_L is the effective first order decay rate in the low K zone. The 1st Damköhler (Da), equal to T_M/T_D, provides a useful indicator of the relative importance of back diffusion on T_{OoM}. Back diffusion impacts are greatest on T_3 when $0.01 > Da > 0.1$, then decrease with increasing Da. Back diffusion has less impacts on T_2, with limited influence on T_1. The results are summarized in a simple conceptual

model to aid in evaluating the impact of back diffusion on the time for concentrations to decline by 1-3 OoM.

Keywords: back diffusion, cleanup time, sensitivity, parameters, Damköhler

1. Introduction

Diffusion can have major impacts on contaminant transport in unconsolidated sedimentary formations when the Darcy velocity in low permeability (K) zones is very small. As a groundwater plume advances downgradient through high K zones, dissolved contaminants are transported by molecular diffusion into low K zones, slowing the downgradient migration of the contaminant plume. However, once the contaminant source is greatly reduced, contaminants diffuse out of low K zones, slowing the cleanup rate in the high K zone (Grisak and Pickens, 1980). This process, termed 'back diffusion', can greatly extend cleanup times following source removal, especially for chlorinated solvents where large reductions in contaminant concentrations are required to meet remediation goals.

The impacts of back diffusion on aquifer cleanup times have been documented in several detailed field studies. Mackay et al. (2000) demonstrated that back diffusion from an underlying clayey aquitard increased the groundwater cleanup time for a pump and treat system enclosed within a sheet-pile test cell. Model predictions based on diffusion of contaminant within the aquitard were consistent with measured concentration profiles (Liu and Ball, 2002). At a DNAPL site in Connecticut, Chapman and Parker (2005) reported that trichloroethylene (TCE) concentrations in downgradient wells declined by roughly 1 Order-of-Magnitude (OoM), when the upgradient source area was isolated with sheet piling. However, after this initial decline, TCE concentrations appeared to plateau or decline more slowly, consistent with back diffusion from an underlying aquitard. Numerical simulations indicate that back diffusion will cause TCE concentrations in downgradient wells to remain above target cleanup levels for centuries. Parker et al. (2008) showed that back diffusion of TCE from the thin low-K beds will significantly delay

groundwater cleanup at a well characterized TCE site in Florida, following complete source isolation with an innovative hydraulic capture system.

The physics of back diffusion and impacts on aquifer cleanup have been examined in several well controlled laboratory experiments. Doner (2008) measured the impacts of back diffusion on aquifer cleanup rate in a 1.07 m long laboratory tank containing a continuous sand body with suspended clay zones. A bromide and fluorescein tracer solution was flushed through the tank for 22 days followed by clean water for 100 days. The lower diffusion coefficient for fluorescein (5.5E-10 m^2/s) compared to bromide (20.1E-10 m^2/s), resulted in more extensive tailing of the fluorescein break-through curve. Yang et al. (2015) measured diffusion driven solute transport between a high K sand and thin low K layers of varying thickness (1.5, 2, and 6 cm) in 0.28 m long laboratory tank experiments with rapid flushing of the high K layer (0.65 pore volumes/day). Mass flux from the low K layer to the high K layer was well described by analytical solutions using the method of images. Tatti et al. (2018) measured back diffusion rates in a 0.68 m laboratory tank containing low K lenses in a continuous high K aquifer. Increasing the solute transport velocity from 5 to 20 m/d increased diffusive flux by more rapidly removing the solute from the high K zone near the low K interface.

The effects of back diffusion on cleanup time can be evaluated using existing analytical (Sale et al. 2008, Farhat et al. 2012) and numerical models. Chapman et al. (2012) demonstrate that high resolution numerical models can accurately simulate the back diffusion process and predict concentration changes over 3 OoM in heterogeneous sand tank experiments (Doner, 2008), when the source condition and low K zone geometry is accurately incorporated in the models.

However, the high concentration gradients near the high/low K interface, require a fine vertical discretization to accurately simulate back diffusion (Farhat et al., 2020).

Muskus and Falta (2018) develop a semi-analytical modeling approach to simulate the effects of diffusion in low K zones on solute concentrations in the more transmissive zones. Contaminant concentration profiles in extensive low K aquitards and finite-thickness embedded low K zones are represented with a fitting function that is adjusted at each timestep. The resulting diffusion fluxes are added to the numerical model as linear concentration-dependent source/sink terms, eliminating the need for fine discretization of the low K region, greatly reducing computation time. Simulation results closely match results from laboratory experiments with layered systems (Yang et al., 2015) and irregularly shaped low K lenses (Doner, 2008), fine grid numerical simulations, and analytical solutions for diffusion in fractured rock and with parent-daughter decay reactions (Muskus and Falta, 2018).

Halloran and Hunkeler (2020) recognize that the interplay between advection, diffusion, sorption and degradation processes will control plume persistence, and use a high-resolution numerical model to examine the impact of simultaneously varying five key input parameters [layer thickness, aquifer K, retardation factor, decay rate (λ), and diffusion coefficient (D_M)], requiring 288 model runs for three different aquifer geometries. To aid in interpreting this large and complex dataset, results are presented in a series of color maps and reduced dimension variables for key performance metrics. Visual evaluation of these results indicates that back diffusion impacts on cleanup time are greatest in thin, confined high K zones with lower groundwater velocity, larger D_m and lower λ.

In summary, physically based analytical and numerical models can reproduce the results of controlled laboratory experiments and well characterized field investigations of back diffusion. The underlying physics indicate that aquifer cleanup times will be controlled by the physical characteristics of both the higher and lower permeability zones [hydraulic gradient (i), permeability (K), porosity (θ), and layer geometry], chemical properties of the contaminant and aquifer material [molecular diffusion coefficient (D_m), effective tortuosity (τ), linear equilibrium retardation factor (R), and effective first order decay rate (λ)], and site characteristics [contaminant loading period (T_L), contaminant source concentration (C_S), remediation goals, and distance to the monitoring or compliance point (X)]. Generating accurate estimates for each of these parameters is an overwhelming challenge at most remediation sites. To effectively apply these models for site management, we must identify the model input parameters that have the greatest impact on simulation results and prioritize characterization resources on those key parameters.

Here, we identify the aquifer, contaminant, and site characteristics that have the greatest impact on the time after complete source removal (T_{OoM}) for contaminant concentrations at a specified compliance point to decline by 1, 2 and 3 Orders-of-Magnitude (OoM). We vary all key input parameters influencing back diffusion over realistic ranges for unconsolidated sedimentary formations, generating a large database of T_{OoM} values. Statistical analysis of this database provides insights into the dominant processes influencing cleanup time after source removal. We demonstrate that T_{OoM} is strongly correlated with characteristic scaling parameters and can be estimated using simple regression models. We identify the aquifer and contaminant

145 characteristics that have the greatest impact on T_{OoM}, and the conditions when individual
146 processes are most important. These results can guide site characterization efforts and aid in
147 interpreting model output for a broad range of site conditions and contaminants.
148

149 ## 2. Approach

150 Numerical simulations are conducted to evaluate the effects of diffusive mass transfer between
151 high and low K zones on the time to reach varying cleanup levels for a range of site conditions.
152 Cleanup time (T_{OoM}) is calculated as the time after complete source elimination for contaminant
153 concentrations to decline by 1, 2 and 3 Orders-of-Magnitude (T_1, T_2 and T_3) in downgradient
154 monitor wells. The contaminant source concentration is assumed to be constant for a loading
155 period, T_L, then completely removed, causing the concentration entering the downgradient
156 aquifer to immediately drop to zero. OoM reductions are calculated based on the contaminant
157 concentration at the well, at the time the source is eliminated. For example, if the concentration
158 in a monitoring well was 5,000 µg/L when the source was eliminated, then T_3 is the time
159 required for the concentration to decline to 5 µg/L, a factor of 1000 reduction, or 3 OoMs.
160

161 The variation in high K zone contaminant concentrations with time is determined using the
162 modeling approach developed by Muskus and Falta (2018) and incorporated in REMChlor-MD
163 (Falta et al., 2018). Advection, dispersion, linear equilibrium sorption, and 1st order decay in the
164 mobile zone are simulated with a finite difference solution to the advection dispersion equation.
165 Diffusion fluxes for each cell are calculated using the semi-analytical approach developed by
166 Muskus and Falta (2018). Groundwater velocity in the low K zone is zero in all simulations.

Mass transfer between the high and low K zones occurs by molecular diffusion with an effective diffusion coefficient (D*)

$$D^* = \tau D_m$$

where D_m is the molecular diffusion coefficient in ground water at the ambient temperature and τ is the tortuosity coefficient. In all simulations, D_m=9.1E-10 m^2/s (0.029 m^2/yr), a representative value for trichloroethylene (Falta et al., 2018). D* is lower than D_m due to increased diffusion distance along tortuous diffusion paths and increased viscosity in narrow pores (Grathwohl, 1998). τ is commonly reported to vary between 0.2 and 0.5 (Grathwohl, 1998; Carey et al., 2016). However, values less than 0.1 have been reported for soils with >25% clay (Ayral and Demond, 2014).

Two aquifer geometries are evaluated (Figure 1): a) layered geometry (LG); and b) boundary geometry (BG). For LG, the embedded low K layers are sufficiently thin such that the average contaminant concentration in the low K zone approaches the average high K zone concentration by the end of the loading period. For BG, the semi-infinite low K boundaries are sufficiently thick that solutes diffusing into this zone do not reach the layer boundary within the simulation period. For the BG, the homogeneous aquifer has a thickness B' and is bounded on one side by a semi-infinite boundary. Monitor wells located a distance X, downgradient of the source, represent the vertically averaged concentration in the high K zone (C_H).

2.1.Typical Simulation Results

Figure 2a shows a typical contaminant break-through curve (BTC) in a monitor well located 100 m downgradient of the source for the boundary geometry (BG). For this example, the high K

190 aquifer is 3 m thick, K=0.02 cm/s, and the monitor well has a 3 m long screen. 1D results (Δx=
191 1 m) are compared with vertically averaged concentrations from two-dimensional (2D) vertical
192 profile simulations (Δx=1 m, Δz=0.1 m) with two different values of vertical dispersivity (α_v).
193 The normalized contaminant concentration (C_H/C_S) is equal to the average contaminant
194 concentration in the high K zone (C_H) divided by the source concentration (C_S). All other
195 parameters are for the base case condition presented in Table 1.
196
197 For both the 1D and 2D simulations (Figure 2a), C_H/C_S increases rapidly, reaching ~1 within a
198 few years, remains high for the 50 yr loading period, and then rapidly declines once the source is
199 eliminated, similar to simulation results by Chapman and Parker (2005). At ~60 yr (10 yr after
200 source removal), there is a slope-break in the C_H/C_S curve, and contaminant concentrations begin
201 to decline more slowly. In this example, C_H/C_S declined by 1 OoM at 56 yr, 2 OoM at 95 yr, and
202 3 OoM at 255 yr, so T_1 = 6 yr, T_2=45 yr, and T_3=205 yr. In most simulations, T_1 occurs before
203 the slope-break and is controlled by advective flushing of the high K zone, while T_3 generally
204 occurs after the slope-break, and is influenced by both the advective flux in the high K zone and
205 the diffusive flux out of the low K zone. T_2 may occur before or after the slope-break, depending
206 on aquifer and site characteristics.
207
208 One dimensional (1D) simulation results (Δx=1 m) closely match vertically averaged
209 concentrations in 2D simulations with vertical dispersivity (α_v) = 0.001 m (normalized root mean
210 square error, NRMSE= 8.9%) and α_v= 0.01 m (NRMSE=4.1%). T_1, T_2 and T_3 differ by 1%, 8%
211 and 6% between the 1D simulation and 2D simulation with α_v = 0.001 m.
212

213 Figure 2b shows concentration profiles for α_v = 0.01 and 0.001 m at T=100 yr and X=100 m.
214 Concentrations are highest immediately adjoining the low K boundary, then decrease rapidly
215 with distance. When α_v < 0.01 m, most contaminant mass is within 2 m of the low K boundary.
216 These results illustrate that 1D simulation results closely approximate 2D results when
217 essentially all contaminants released from the low K boundary remain within the screened
218 interval of the monitoring well (i.e., B' = monitor well screened interval). Increasing the aquifer
219 thickness to greater than 3 m, reduces the vertically averaged concentration by dilution with
220 uncontaminated water. In the sensitivity analyses, 1D simulations with a maximum aquifer
221 thickness of 3 m to reduce computation times.
222

223 ## *2.2. Sensitivity Analysis Database*

224 Model input parameters evaluated in the sensitivity analysis are presented in Table 1. A 'base
225 case' set of simulations is first conducted where K_H, X, f, n_L and B' are varied to reflect the
226 effects of aquifer geometry on T_{OoM}, generating 840 individual values of T_1, T_2 and T_3. Each
227 base case simulation is then repeated for each value of θ_H, θ_L, R_H, R_L, τ, T_L, and λ_L shown in
228 Table 1. When the T_{OoM} is greater than the 1,000 yr simulation period, these values are excluded,
229 resulting in a total of ≈21,000 individual values of T_1, T_2 and T_3 for use in the regression
230 analyses. Statistical moments for parameters in the dataset without decay (λ_L =0) are
231 summarized in Tables S-1 for LG and S-2 for BG. Many of the key indicator parameters are log
232 normally distributed, and so Ln transformed values are also presented.
233

234 Table 1. Parameter values for base case simulations and sensitivity analysis

Parameter	Symbol	Base Case	Sensitivity Analysis
Hydraulic gradient, m/m	i	0.001	--
Longitudinal dispersivity, m	α_L	1.0	--
Molecular diffusion coefficient, m^2/s	D_m	9.1E-10	--
High K permeability, cm/s	K_H	0.01, 0.02, 0.03, 0.05, 0.1	--
Distance from source, m	X	25, 50, 75, 100, 125, 150	--
High K volume fraction	f	0.1, 0.2, 0.4, 0.6, 0.8, 0.9	--
Number of low K layers	n_L	1, 2, 3, 4	--
LG aquifer thickness, m	B	3	
BG aquifer thickness, m	B'	0.5, 1, 2, 3	--
Loading period, yr	T_L	50	10, 25, 100
Tortuosity coefficient	τ	0.7	0.07, 0.35
High K retardation factor	R_H	1	2, 5, 10
Low K retardation factor	R_L	1	2, 5, 10
High K porosity	θ_H	0.3	0.15, 0.45
Low K porosity	θ_L	0.3	0.15, 0.45
Low K decay rate, 1/yr	λ_L	0	0.001, 0.01, 0.1, 1

235

236 For BG, preliminary results showed that T_{OoM} values are identical for an aquifer of thickness B'
237 with one low K boundary and an aquifer of thickness 2B' with two low K boundaries, so the
238 number of boundaries is not varied. The BG aquifer thickness (B') is varied from 0.5 to 3 m. For
239 LG, the parameters X, f, and n_L are varied to reflect the effect of aquifer geometry on T_{OoM}. For
240 LG, the aquifer thickness (B) is constant at 3.0 m, equivalent to the length of common monitor
241 well screens. The LG aquifer contains n_L low K layers of thickness $2L_D=B(1-f)/n_L$ where f is the
242 volume fraction of the high K zone, so low K layer thickness varies between 0.075 and 2.7 m.

For both LG and BG, X and K_H were varied to cover a broad ranges of site conditions, so the datasets also include some extreme values. For example, the high K zone non-reactive travel time (T_t) to the monitoring or compliance point varies from 0.1 to 21 yr. While this range is physically plausible, it is unlikely that a compliance point would be established 0.1 or 21 yr travel time away from the source. By including some extreme values in the dataset, we ensure the regression relationships accurately reflect model behavior for a broad range of conditions.

For both LG and BG, a fifty-year loading period (T_L) is selected for the base case, which is equivalent to a spill occurring in 1970 with complete (100%) source removal in 2020. In the sensitivity analysis, T_L values of 25 and 100 yr are also evaluated. The transverse dispersivity equal to zero in all simulations to eliminate the effects of transverse dispersion. The longitudinal dispersivity, α_L, is constant at 1 m, allowing limited longitudinal dispersion (Zech et al., 2015).

2.3. Scaling Parameters

To assist with interpretation of the modeling results, we identify a set of scaling parameters for a unit-width aquifer, based on the geometry of the high and low K zones, distance from the source to the monitoring point (X), high K porosity (θ_H), low K porosity (θ_L), high K retardation factor (R_H), and low K retardation factor (R_L). Characteristic time scales include the high K travel time (T_t), hydraulic retention time (T_H), mass retention time (T_M), and loading period (T_L). T_t, T_H and T_M in years are defined as

$$T_t = PV_H/Q$$

$$T_H = (P_{VH} + P_{VL})/Q$$

$$T_M = (R_H P_{VH} + R_L P_{VL})/Q$$

based on the high K pore volume (P_{VH}), low K pore volume (P_{VL}), and volumetric discharge per unit width through the aquifer (Q). Characteristic scaling ratios include the ratio of low K to high K zone thickness (α), ratio of low K to high K pore volume (β) and ratio of low K to high K contaminant mass storage (γ), defined at the end of the loading period (T_L).

For LG, the characteristic diffusion length (L_D) is equal to half the low K layer thickness and is independent of time, allowing us to calculate a characteristic diffusion time (T_D) where $T_D = R_L L_D^2/4D^*$. For the BG, the volume of the contaminated low K zone will increase over time, as contaminants diffuse deeper into the semi-infinite low K boundary, so L_D will increase with T_L. For BG, we define $T_D = T_L$ and

$$L_D = \frac{\text{Mass stored in low K boundary at end of loading period } T_L}{\text{Source concentration} * R_L * \theta_L * \text{width} * X}$$

In Supporting Information (Figure S-1), we show that for $T_L > 0.75\ R_H\ T_t$, L_D can be estimated using the relationship $L_D = (4.73\ (T_L - 0.75\ R_H\ T_t)\ D^*/R_L)^{0.5}$.

The 1st Damköhler number is a dimensionless parameter used to relate reaction rates to transport rates. In this work, we define Da as T_M/T_D. Characteristic time and length scales for LG and BG are defined in Table 2.

291

292 Table 2. Definition of characteristic time and length scales

Parameter	Symbol	LG Definition	BG Definition
Discharge (m^2/yr)	Q	$K_H f\ B\ i$	$K_H B'\ i$
High K travel time (yr)	T_t	$X\theta_H / K_H i$	
Hydraulic retention time (yr)	T_H	$\frac{X(\theta_H f + \theta_L(1-f))}{K_H f i}$	$\frac{X(\theta_H B' + \theta_L L_D)}{K_H B' i}$
Mass retention time (yr)	T_M	$\frac{X(R_H\theta_H f + R_L\theta_L(1-f))}{K_H f i}$	$\frac{X(R_H\theta_H B' + R_L\theta_L L_D)}{K_H B' i}$
Diffusion Time (yr)	T_D	$R_L L_D^2 / 4D^*$	T_L
Diffusion Length (m)	L_D	$B(1-f) / 2n_L$	$\left(\frac{4.73(T_L - 0.75R_H T_t)D^*}{R_L}\right)^2$
Low to high K thickness ratio	α	$\frac{(1-f)}{f}$	L_D/B’
Low to high K pore volume ratio	β	$\frac{\theta_L(1-f)}{\theta_H f}$	$\theta_L L_D / (\theta_H B')$
Low to high K mass ratio	γ	$\frac{R_L\theta_L(1-f)}{R_H\theta_H f}$	$\frac{R_L\theta_L L_D}{R_H\theta_H B'}$
1st Damköhler number	Da	T_M/T_D	

293

294 Box-whisker plots showing the distribution of the scaling parameters for LG and BG datasets
295 without decay (λ_L=0) are shown in Figure 3. For LG, median advection times (T_t, T_H, T_M) vary
296 from 2 to 8 yr, while median cleanup times vary from 12 yr for T_1 to 37 yr for T_3. The relatively
297 narrow range between the median 1 and 3 OoM cleanup time, implies that mass transfer is often
298 relatively rapid for the layered geometry, which is consistent with the relatively short median

299 diffusion time (T_D) of 1.4 yr. Median advection times (T_t, T_H, T_M) for BG vary from 2 to 8 yr,
300 similar to the embedded geometry. However, median cleanup times for BG are much more
301 variable, ranging from 5 yr for T_1 to 217 yr for T_3. The large difference between 1 and 3 OoM
302 cleanup times for BG, implies that diffusive mass transfer is often slow relative to advection.
303 The largest difference between the LG and BG datasets is for T_D. For LG, T_D varied from 0.02
304 to 227 yr, causing Da (T_M/T_D) to vary by 5 OoM. For BG, T_D varied from 25 to 100 yr, causing
305 Da to vary over a narrower range (0.004 to 5).
306

307 ## 3. Results and Discussion

308 ### *3.1. Base Case Simulations*

309 Figure 4 shows selected results from the REMChlor-MD simulations for the base case conditions
310 for LG and BG. T_{OoM} is a function of the hydraulic retention time (T_H) and diffusion length (L_D)
311 for LG, and a function of the T_H and B' for BG. Note that for the base case conditions, R_H=R_L=1,
312 so T_M=T_H for both LG and BG. The data points for each curve are individual simulation results
313 for X between 25 to 150 m and K_H between 0.01 and 0.1 cm/s. For constant values of L_D and B',
314 the points plot on a smooth curve indicating X and K_H are not important predictors of T_{OoM}.
315

316 For the base case LG, the time to 1 OoM cleanup (T_1) varies approximately linearly with T_H, and
317 is relatively insensitive to L_D, indicating diffusive transport between high and low K zones is not
318 the primary control on cleanup time for the 1st OoM reduction. T_2 and T_3 also vary with T_H, but
319 are more sensitive to L_D, indicating the diffusive transport becomes more important when larger
320 OoM reductions are required. For larger T_H, T_2 and T_3 are linear functions of T_H, implying
321 advective transport controls cleanup time. However, for smaller T_H, T_2 and T_3 increase much

more rapidly with T_H, consistent with solute diffusion between high and low K zones influencing cleanup time.

For the base case BG, T_1, T_2 and T_3 are primarily controlled by T_H, and, to a lesser extent, B'. Similar to the layered geometry, T_1 increases approximately linearly with T_H, indicating cleanup is controlled by advective transport. T_2 and T_3 increase approximately in proportion to the square root of T_H and increase with smaller values of B' as diffusive flux from the low K boundary becomes more significant relative to advective flux in the high K zone.

3.2. Parameter Sensitivity

The results presented above illustrate that cleanup time is due to complex interactions between advective and diffusive transport processes. Traditional sensitivity analyses, where a single parameter is varied while all others remain constant, may not reveal the complex interactions that can occur. To provide a more robust evaluation of parameter sensitivity, the distribution of T_{OoM} values for the base case is compared with T_{OoM} distributions for each value of θ_H, θ_L, R_H, R_L, τ, T_L, and λ_L. To aid in interpreting these results, box-whisker plots are presented showing the median value, 25%/75% quartiles, and 5%/95% limits of the T_{OoM} distribution for several important parameters (Figure 5). For presentation in Figure 5, T_{OoM} values greater than 1000 yr are entered as 1000 yr.

In general, the time to reach 1 OoM cleanup (T_1) is relatively insensitive to most model parameters for both LG and BG. This is likely due to the relatively minor impacts of back diffusion on T_1. In contrast, model parameters have a much greater impact on T_3, since T_3 is

much more strongly influenced by back diffusion. T_3 is often much greater for BG, than LG, indicating back diffusion is a much more important process in aquifers with thick low K boundaries.

Increasing contaminant loading period (T_L) results in variable impacts on cleanup time. For LG, increasing T_L results in minor increases in T_1, T_2, and T_3. For BG, increasing T_L results in substantial increases in T_3, but variable impacts on T_1 and T_2. For BG, longer T_L results in greater penetration of contaminants into the low K boundary and increases the duration of back diffusion. For LG, the characteristic diffusion time (T_D) is often less than T_L, so further increases in T_L do not have a substantial impact on the T_{OoM} distributions.

Changes in tortuosity (τ) have a complex relationship with T_{OoM}. For the base case simulations, τ=0.7 and D*=0.02 m^2/yr. Reducing τ to 0.07, reduces D* to 0.002 m^2/yr, increasing T_D for LG by 3.16 ($10^{0.5}$). In some LG cases, an increase in T_D can shift the process from advection dominated to diffusion dominated, increasing T_{OoM}. For BG, reducing τ by a factor of 10, reduces L_D by a factor of 3.16, which leads to a reduction in the mass stored in the low K boundary, reducing cleanup time.

Changes in the low K retardation factor (R_L) can also have unexpected impacts on T_{OoM}. For LG, increasing R_L corresponds with an increase in T_1, T_2, and T_3, with the largest impact on T_3. However, for BG, increasing R_L corresponds with more modest increases in T_1, T_2 and T_3, with the least impact on T_3. The limited impact on T_3 is related to the reduced diffusion length (L_D) with larger R_L.

368

369 Changes in the low K porosity (θ_L) have a more consistent impact on T_{OoM}. Increasing θ_L
370 increases the mass stored in low K zones for LG, increasing T_1, T_2 and T_3. For BG, increasing
371 θ_L results in an increase in T_3, but has very limited impacts on T_1.

372

373 Increases in the low K contaminant decay rate (λ_L) for LG result in minor reductions in T_1, with
374 somewhat greater reductions for T_2 and T_3. For BG, increasing λ_L has minor impacts on T_1,
375 greater impacts on T_2, and can result in very large reductions in T_3, especially for λ_L=1/yr. The
376 much greater impact of λ_L on T_3 for LG is due to the much greater impact of back diffusion on
377 cleanup time for this geometry.

378

379 ### *3.3. Scaling Parameter Analysis*

380 Results from the base case simulations and sensitivity analysis show that back diffusion has a
381 much greater impact on T_3 than T_1, and the ratio T_3/T_1 is large when back diffusion has a major
382 influence on T_{OoM}. In Figure 6, T_3/T_1 is plotted versus the first Damköhler number (Da) for both
383 LG and BG with no decay (λ_L =0). Note that at an individual site, T_D is constant, so Da
384 increases linearly with distance from the source.

385

386 The ratio T_3/T_1 is very sensitive to Da, varying over 2 OoM. In a small number of BG cases near
387 the source when velocity is high (Da<0.01), T_3/T_1 is reduced indicating limited impacts of back
388 diffusion. With increased travel time (lower K_H and/or larger X), T_3/T_1 increases, reaching a
389 maximum in the range 0.01<Da<0.1, for both LG and BG. For LG, T_3/T_1 declines as Da
390 increases, eventually approaching 1 for very large Da. A similar pattern appears to occur for

391 BG. However, the range of Da in the BG dataset is much smaller, so it is not possible to
392 determine if T_3/T_1 continues to decline for large values of Da.
393
394 A correlation analysis was conducted to identify relationships between different scaling
395 parameters and T_{OoM}. Table 3 shows correlation coefficients (r) between Ln T_{OoM} and scaling
396 parameters for both geometries with no decay (λ_L =0). For LG, Ln T_1 is strongly correlated with
397 Ln T_M, and weakly correlated with Ln T_D, implying that T_1 is primarily controlled by advective
398 flushing. For LG, the correlation between Ln T_M and Ln T_2 and Ln T_3 is reduced, while the
399 correlation with Ln T_D increases, indicating diffusion is a more important influence on cleanup
400 time for large OoM reductions. For BG, Ln T_{OoM} is strongly correlated with Ln T_M for 1, 2 and 3
401 OoM, indicating the advective flux is a major influence for all cleanup levels. Ln T_D is a poor
402 predictor of Ln T_{OoM} for BG, possibly due to the relatively limited range of T_D considered here
403 (25 to 100 yr). Note that Ln γ is a better predictor of Ln T_{OoM} and γ is a function of T_D. For BG,
404 Ln Da is strongly correlated with Ln T_{OoM}, because it is strongly correlated with T_M (r=0.99).
405
406 Table 3. Correlation coefficients (r) between scaling parameters and cleanup times for layered
407 and boundary geometries.
408

	Layered Geometry (LG)			**Boundary Geometry (BG)**		
	Ln T_1	**Ln T_2**	**Ln T_3**	**Ln T_1**	**Ln T_2**	**Ln T_3**
Ln T_t	0.61	0.43	0.32	0.79	0.72	0.67
Ln T_H	0.87	0.79	0.70	0.84	0.86	0.84
Ln T_M	0.98	0.91	0.83	0.96	0.92	0.89
Ln T_D	0.50	0.78	0.87	0.00	0.04	0.15
Ln α	0.57	0.72	0.75	0.25	0.35	0.35
Ln β	0.56	0.70	0.72	0.21	0.37	0.38
Ln γ	0.60	0.74	0.76	0.10	0.45	0.49
Ln Da	0.20	-0.17	-0.34	0.95	0.91	0.85

The impact of T_M on cleanup time is illustrated in Figure 7, where T_{OoM} is plotted versus T_M and T_{OoM}/T_M is plotted versus Da, for both LG and BG with no decay (λ_L =0). The strong correlation between T_{OoM} and T_M is evident for both LG and BG. By dividing T_{OoM} by T_M, we eliminate the primary impact of advective flushing, and can look for secondary impacts of diffusion limited mass transfer.

For LG, the ratio of T_{OoM}/T_M varies with Da, and can be separated into three regions. When Da is very large (>100), diffusive mass transfer from the low K zone to the high K zone is rapid relative to advection, T_1/T_M, T_2/T_M, and T_3/T_M all decline to less than 1.5, similar to values predicted by the advection-dispersion equation (ADE) with α_L=1 m (ADE results not shown). When Da<0.1, T_1/T_M and T_2/T_M are highly variable, and small values occur under certain conditions. We hypothesize that for small Da, the average concentration in the high K zone approaches zero, the low K concentration gradient and diffusive flux reach a maximum, and further increases in the advective flux only dilutes contaminants released from the low K zone, reducing time to reach 1 and 2 OoM reductions. Between the extreme behavior observed for very high and very low Da, cleanup time is influenced by both advection in the high K zone and diffusion in the low K zone. The maximum values of T_2/T_M and T_3/T_M occur for Da<0.01, then decrease as Da increases. As discussed below, it is not possible to fit a single function to the full range of Da.

For BG, T_D=T_L, so T_D varies over a relatively narrow range (25 to 100 yr), and Da is generally less than 1. T_1/T_M generally varies between 0.3 and 3, and does not correlate with Da. T_3/T_M

433 may be low for very small Da, reaches a maximum near Da~0.01, then decreases steadily with
434 increasing Da. When Da<0.01, T_3 can occur before the break in slope shown in Figure 2, when
435 cleanup time is controlled by advective flushing only. When Da>0.01, T_3 is always in the slowly
436 declining portion of the flush-out curve, after the slope break, when cleanup time is influenced
437 by both the advective flux in the high K zone and the diffusive flux out of the low K zone. In the
438 database, T_2 occurs before the slope break in about 15% of the simulations, resulting in low
439 values of T_2/T_M. For the remainder of the database where T_2 occurs after the break in slope,
440 T_2/T_M is higher and more variable.
441
442 ### *3.4. Regression Analysis*
443 A regression analysis is performed using JMP Pro (Sall et al., 2017) to identify the independent
444 variables that have the greatest influence on cleanup time and develop simplified relationships to
445 aid in interpreting both field characterization and simulation results. Preliminary analyses
446 indicate that most of the model input parameters are correlated with cleanup time ($p<0.01$), and
447 their inclusion in the regression model would improve precision. However, interpreting a
448 complex regression model with multiple, sometimes poorly characterized inputs can be
449 challenging. In this work, regression models are developed with the minimum number of inputs
450 that provide an acceptable estimate of cleanup time. 'Acceptable' is judged against the typical
451 uncertainty in aquifer characteristics at remediation sites.
452
453 T_{OoM} can be estimated using equation 1a for the LG and equation 1b for BG.

454 $$\text{Ln } T_{OoM} = C_1 + C_2 \text{ Ln } T_M + C_3 \text{ Ln } T_D \quad (1a)$$

455 $$\text{Ln } T_{OoM} = C_1 + C_2 \text{ Ln } T_M + C_3 \text{ Ln } \gamma \quad (1b)$$

where T_M is the mass residence time, T_D is the diffusion time, and γ is the ratio of the low K to high K contaminant mass. Ordinary linear regression estimates of C_1 to C_3 are presented in Table 4 for the LG and BG. Also included in Table 4 are the standard error of the estimate (SE) for each coefficient, the coefficient of determination (r^2), root mean squared error (RMSE), and the 90% confidence interval (CI) of the ratio $T_{regress}/T_{REMCHlor}$. It is not possible to fit a single relationship to the full range of Da for LG. LG regression coefficients are presented for T_1 for Da>1 and for T_2 with Da>0.1. By limiting regression dataset to Da greater than the threshold, we eliminate data points close to the source, where back diffusion does not exert a major influence on cleanup time, and T_1 and T_2 are less than 10 yr.

Table 4. Regression coefficients and goodness of fit statistics for layered and boundary geometry.

	Layered Geometry (LG)			**Boundary Geometry (BG)**		
	1 OoM	**2 OoM**	**3 OoM**	**1 OoM**	**2 OoM**	**3 OoM**
Da Range	Da>1	Da>0.1	All Da	All Da	All Da	All Da
C_1	0.671 ±0.004	1.705 ±0.004	2.317 ±0.004	-0.430 ±0.014	1.026 ±0.017	3.925 ±0.008
C_2	0.936 ±0.002	0.692 ±0.002	0.554 ±0.002	1.123 ±0.006	1.231 ±0.007	0.685 ±0.004
C_3	0.105 ±0.001	0.306 ±0.001	0.428 ±0.001	-0.192 ±0.006	0.313 ±0.007	0.248 ±0.004
r^2	0.987	0.977	0.974	0.936	0.929	0.943
RMSE	0.170	0.216	0.230	0.340	0.409	0.196
n	11,517	13,982	13,984	2,583	2,571	2,462
90% CI	0.76-1.32	0.70-1.43	0.68-1.46	0.57-1.75	0.51-1.96	0.72-1.38

Cleanup times calculated with REMChlor-MD and Eq 1 (Regress T_{OoM}) for LG and BG are compared in Figure 8. Eq. 1 explains 97-99% in of the variation in Ln T_{OoM} for LG and 93-94% of the variation for BG. 90% of the regression estimates are within a factor of 2 of the

474 REMChlor-MD results of T_1, T_2 and T_3 for both LG and BG. For LG, Eq. 1 may overestimate
475 T_1 for Da<1 and T_2 for Da<0.1.
476
477 Note that in Eq 1, T_M, T_D and γ reflect the collective influence of D_m, τ, K_H, X, f, n_L, B', θ_H, θ_L,
478 R_H, and R_L, on T_{OoM}. Interestingly, the impact of contaminant loading time T_L is different
479 between the two considered low K geometries. For BG, T_L is incorporated in the T_M and γ
480 terms. For LG, addition of T_L improved r^2 by less than 0.0005, and T_L was not included in the
481 final regression model. The limited impact of T_L on cleanup time is not surprising since the
482 median value of T_D is 1.4 yr for LG. When $T_L>T_D$, the high K and low K layers will approach
483 equilibrium and changes in T_L will have little impact on T_{OoM}.
484
485 Ln T_t and Ln T_H are also correlated with Ln T_{OoM} (Table 3), and regression equations could be
486 developed based on these time parameters. However, T_M provides the best prediction when there
487 are significant variations in θ and R. Note that when $R_H=R_L=1$, $T_M=T_H$.
488
489 The impacts of T_M and T_D on T_{OoM} are illustrated in Figure 9a for LG, downgradient from the
490 source where Da is within the allowable range for the regression equations. T_{OoM} is calculated
491 with Eq. 1a for T_D = 0.03, 1.4, and 45 yr which correspond to the 5, 50, and 95 percentile values
492 of T_D in the database. T_1 is not plotted for T_D=45 yr, because Da<1 and the regression equation
493 for T_1 is less accurate in this region. Downgradient of the source (T_M>5 yr), T_1, T_2 and T_3
494 increase nearly linearly with T_M. Order of magnitude increases in T_D, result in substantial
495 increases in T_2 and T_3, similar to results observed for the base case simulations (Figure 4).
496

497 For the BG, Figure 9b shows plots of T_{OoM} versus T_M generated with Eq. 1b for γ = 0.3, 1.5 and
498 6.8 which correspond to the 5, 50, and 95 percentile values of γ in the dataset. Similar to the
499 base case results (Figure 4), T_1 increases linearly with T_M and is relatively insensitive to γ. T_3
500 increases much more rapidly with T_M and is more sensitive to γ, resulting in very long cleanup
501 times for large values of γ. Cleanup times increase when contaminants diffuse deep into the low
502 K boundary prior to source removal (long T_L, large D*, low R_L) or when Q is small. These
503 results are consistent with numerical simulation results by Halloran and Hunkeler (2020) who
504 found that diffusive mass transport with low K zones had the greatest impact on concentrations
505 in monitor wells when Darcy velocity and B' are small or D* is large.
506
507 *3.5. Decay in Low K Zones*
508 Sensitivity analyses were conducted to evaluate the impact of variations in the 1st order decay
509 rate in the low K zone (λ_L) on T_{OoM}. λ_L was varied between 0.001 and 1 per yr (half-life between
510 690 and 0.69 yr). The cleanup time ratio for decay (CTR_λ) is used to evaluate the impact of λ_L
511 on T_{OoM} while keeping all other parameters identical.
512 $$CTR_\lambda = T_{OoM} \text{ for } \lambda_L>0 \; / \; T_{OoM} \text{ for } \lambda_L=0 \qquad (2)$$
513 Sensitivity analysis results reveal that reductions in CTR_λ are a function of $\lambda_L T_D$. Figure 10
514 shows CTR_λ plotted versus $\lambda_L T_D$ for LG and BG. For both LG and BG, decay has minor impact
515 on T_{OoM} when $\lambda_L T_D<0.01$. Under certain conditions, the impacts of degradation on CTR_λ can be
516 estimated with the relationship Ln $CTR_\lambda = C_4 + C_5$ Ln ($\lambda_L T_D$). Ordinary linear regression
517 estimates for C_4 and C_5 and goodness of fit statistics are presented in Table 5. For T_3 (both LG
518 and BG) and T_2 (LG only), the regressions provide reasonably precise estimates of Ln CTR_λ
519 (RMSE= 0.24-0.26) for T_2 and T_3 when $\lambda_L T_D>0.01$. For T_1 (both LG and BG), and T_2 (BG

520 only), the regressions provided a relatively poor fit to the data and coefficients are not included
521 in Table 5.
522
523 Table 5. CTR_λ regression coefficients and goodness of fit statistics.

	Layered Geometry (LG)		**Boundary Geometry (BG)**
	2 OoM	**3 OoM**	**3 OoM**
$\lambda_L T_D$ Range	>0.01	>0.01	>0.01
Da Range	Da>0.1	All Da	All Da
C_4	-1.182 ±0.007	-1.262 ±0.008	-1.514 ±0.011
C_5	-0.486 ±0.004	-0.538 ±0.005	-0.536 ±0.004
r^2	0.911	0.918	0.928
RMSE	0.242	0.255	0.392
n	1,219	1,219	1,380
90% CI	0.67-1.49	0.66-1.52	0.52-1.91

524
525 Contaminant decay in low permeability zones can occur through both biotic and abiotic
526 processes. Based on compound specific isotope analysis, λ_L values for TCE degradation were
527 reported to vary between 0.03 and 8.75/yr in an aquitard in Borden, Ontario, Canada (Wanner et
528 al., 2016) and between 0.1 and 0.15/yr in a thin clayey aquitard in Florence, SC, USA (Wanner
529 et al., 2018). Schaefer et al. (2018) reported λ_L values between 0.0002 and 0.04/yr for abiotic
530 reduction of TCE in low K unconsolidated sediments, with higher rates in sediments with more
531 organic carbon and reduced iron. Given typical values for T_D in LG and BG systems, reported
532 decay rates are sufficient to substantially reduce cleanup times in many systems.

533

534 ### *3.6. Regression Model Evaluation*

535 Chapman and Parker (2013) present results from high resolution numerical simulations of
536 forward and back diffusion for conditions equivalent to the LG and BG geometry for different
537 values of R_L, λ_L and X. Figure 11 presents a comparison of T_1, T_2 and T_3 values from Chapman
538 and Parker (2013) and this work. T_{OoM} values were estimated using Eq. 1 for Da within
539 allowable ranges. When $\lambda_L>0$, cleanup times were adjusted for decay using Eq. 2. Overall, the
540 regression equations provide reasonably accurate estimates of T_{OoM} for both geometries with r^2=
541 0.80 and normalized RMSE = 0.44 for pooled data. The regression equations appear to slightly
542 over-estimate T_3 for BG and underestimate T_3 for LG. However, all regression estimates are
543 within a factor of two of the Chapman and Parker values. Additional testing is needed to
544 evaluate the regression model performance for a wider range of conditions.

545

546 ### *3.7. Field Examples*

547 Results developed above are applied to two intensively characterized field sites, where TCE was
548 released to the subsurface, resulting in extensive contaminant plumes. Following source area
549 isolation, TCE concentrations decline at both sites, but more slowly than would be predicted
550 based on advection, dispersion and linear equilibrium sorption.

551

552 #### *3.7.1. Low K Layered Geometry*

553 Parker et al. (2008) document the impacts of thin low K layers on cleanup time in a series of
554 monitor wells located 40 m downgradient from where a TCE plume was intercepted by a
555 groundwater extraction, treatment, and reinjection system. Most contamination is present in a

556 sandy zone containing thin low K clay layers. Porosity and linear equilibrium retardation factors
557 were reported to be 0.35 and 1.6 for the high K zone and 0.4 and 3.9 for the low K zone,
558 respectively (Parker et al., 2008). The non-reactive transport velocity in the high K zone (V_H)
559 was estimated to range between 29 and 117 m/yr based on a mass balance analysis and slug test
560 results (Parker et al., 2008).
561
562 In our analysis, the screened interval of the monitor well is represented as a 3 m thick
563 heterogeneous aquifer with one 0.5 m thick embedded low K layer (f=0.83, L_D=0.25 m).
564 Assuming D*= 0.009 m^2/yr, the characteristic diffusion time (T_D) is ~6.9 yr. The relatively large
565 T_D is due to the high value of R_L, slowing mass transfer. At 40 m downgradient, T_M is between
566 0.7 and 2.9 yr, and Da is between 0.1 and 0.4. Estimated cleanup times based on Eq. 1 are T_1= 2
567 to 6 yr, T_2 = 8 to 21 yr, and T_3= 19 to 42 yr. Monitoring results presented by Parker et al. (2008)
568 and Geosyntec (2020) show that TCE gradually declined in monitor wells located 40 m
569 downgradient of the groundwater reinjection system, reaching 1 OoM cleanup levels in 2 to 10
570 yr and 2 OoM in 9 to over 18 yr, consistent with Eq. 1 estimates. These wells have not yet
571 reached the 3 OoM cleanup level, so it is not possible to directly compare T_3 estimates.
572 Uncertainty in T_{OoM} is primarily due to uncertainty in the groundwater velocity and low K
573 retardation factor.
574

575 ### *3.7.2. Low K Boundary Geometry*

576 Chapman and Parker (2005) document the results of back diffusion on aquifer cleanup time in a
577 minimally heterogeneous aquifer underlain by a 20 m thick clayey silt aquitard. The TCE source
578 area was isolated with a sheet piling barrier, approximately 42 yr after the initial release. Porosity

579 and linear retardation factor were reported to be 0.35 and 1.2 for the high K zone, and 0.43 and
580 1.2 for the low K aquitard, respectively. Non-reactive travel time (T_t) to two monitor wells
581 (MW-01 and MW-54) located 330 m downgradient was estimated to be ~1.6 yr based on lab
582 permeameter testing, slug tests and borehole dilution tests. Within the sheet pile enclosure, TCE
583 had migrated almost 3 m into the aquitard, with the 50% break-through point at approximately
584 1.2 m below the aquitard interface. The measured profiles matched simulation results with D*=
585 0.009 m^2/yr (Chapman and Parker, 2005)
586
587 Assuming, a loading period (T_L) of 42 yr and D*=0.009 m^2/yr, the estimated value of L_D is 1.2
588 m, similar to the 50% break-through point observed by Chapman and Parker (2005). For MW-
589 01 which has a 1.5 m long well screen, B'=1.5 m, γ=0.8, T_M= 3.8 yr, Da=0.09, T_1= 3 yr, T_2 = 13
590 yr, and T_3 = 119 yr. For MW-54 which has a 3 m well screen, B'=3.0 m, γ =0.4, T_M= 2.9 yr,
591 Da=0.07, T_1=2.5 yr, T_2=8 yr, and T_3=83 yr. Monitoring results reported by Chapman and Parker
592 (2005) show TCE concentrations declined by about 1 OoM in 3 yr after source isolation,
593 followed by a slower tailing period where concentrations were stable or declined very slowly,
594 which is generally consistent with the Eq. 1 estimates. Neither well MW-01 or MW-54 had
595 reached 2 or 3 OoM cleanup levels, so it is not possible to directly compare cleanup time
596 estimates. The greatest source of uncertainty in the Eq. 1 estimates is the variation in TCE
597 concentration over time, prior to source isolation. Monitoring and modeling results by Chapman
598 and Parker (2005) indicate that TCE concentrations were highest shortly after the initial release,
599 then declined over time, as the source area was depleted by natural flushing. In our analysis, the
600 source concentration is assumed constant for the entire loading period, so estimated
601 concentrations will decline more rapidly than in the field.

602

603 4. Conceptual Model and Conclusions

604 A simplified conceptual model (CM) is proposed to aid site managers in evaluating the impact of
605 back diffusion in unconsolidated sedimentary formations on the time after complete source
606 removal for contaminant concentrations in monitor wells to decline by 1, 2 and 3 OoM (T_{OoM}).
607 While models that simulate the underlying physical processes can provide quantitative estimates
608 of T_{OoM}, implementation of these models requires significant resources for site characterization,
609 high resolution model development, calibration, and interpretation of simulation results. Our
610 CM allows site managers to quickly evaluate if back diffusion substantially increases cleanup
611 time at their site, by how much, and what site characterization information is most important for
612 estimating cleanup time.
613
614 In the CM, the contaminated aquifer is represented by three key parameters: (1) mass residence
615 time (T_M); (2) diffusion time (T_D); (3) ratio of low K to high K contaminant mass storage (γ). T_M
616 is equal to the total contaminant mass stored in high and low K zones divided by the
617 downgradient mass flux. For the layered geometry (LG), T_D is calculated as $T_D = R_L L_D^2/4D^*$
618 where R_L is the low K retardation factor, L_D is half the thickness of the low K layers, and D* is
619 the effective diffusion coefficient. For the boundary geometry (BG), $T_D = T_L$, $L_D = (4.73 (T_L -$
620 $0.75 T_t) D^*/R_L)^{0.5}$ and $\gamma = R_L \theta_L L_D / (R_H \theta_H B')$. All parameters are calculated at the end of the
621 contaminant loading period (T_L).
622
623 T_{OoM} is influenced by both advection in the high K zone and diffusion out of the low K zone.
624 More rapid advective flushing (smaller T_M), reduces the contaminant concentration in the high K

625 zone, increasing the concentration gradient and diffusive mass flux out of the low K region,
626 reducing T_3. More rapid diffusion (lower T_D) increases advective flushing efficiency, reducing
627 T_3.
628
629 The 1st Damköhler (Da) is equal to T_M/T_D and provides a useful indicator of the relative
630 importance of back diffusion on T_{OoM}. Back diffusion has the greatest impacts on T_3 when
631 $0.01>Da>0.1$ with T_3/T_M varying generally between 20 and 100, then decreases with increasing
632 Da. Back diffusion has less impacts on T_2, with limited influence on T_1. When Da is very large,
633 diffusion is fast relative to advection, back diffusion does not substantially increase cleanup time,
634 and T_{OoM} calculated with REMChlor-MD approach values calculated with the traditional
635 advection dispersion equation (ADE).
636
637 Our simplified CM has important similarities with the power law model for source area treatment
638 (Parker and Park, 2004; Falta et al., 2005)
639 $$C_t/C_0 = (M_t/M_0)^{\Gamma}$$
640 where C_t is the time-dependent average contaminant concentration leaving the source zone, C_0 is
641 the initial concentration leaving the source zone, M_t is the time-dependent mass in the source
642 zone, M_0 is the initial mass in the source zone, and the exponent Γ is a fitting parameter that
643 determines the shape of the discharge vs. mass curve. When $\Gamma<1$ or Da is large, effluent
644 concentrations remain high until most contaminant mass is removed, similar to conventional
645 ADE behavior. When $\Gamma>1$ or Da is small, effluent concentrations drop rapidly at first while
646 substantial contaminant mass remains, then decline more slowly, resulting in extensive tailing of

647 the flush-out curve. When $\Gamma \approx 1$ or $Da \approx 1$, effluent concentrations decline in proportion to the
648 mass removed, similar to a continuously stirred tank reactor.
649
650 The CM allows some generalizations about the effects of back diffusion on cleanup time for LG
651 and BG.
652 1. Back diffusion has limited impacts on T_1.
653 2. For LG, T_D is commonly smaller than T_M ($Da > 1$), mass transfer between low K and high
654 K zones is more rapid than advective flushing, and back diffusion will have less impacts
655 on cleanup time.
656 3. For LG, T_M is a function of the total discharge (Q) per unit width through the aquifer, and
657 does not require precise estimates of the high K fraction (f) of the aquifer.
658 4. For BG, $T_D = T_L$, T_D is commonly greater than T_M ($Da < 1$), and back diffusion may
659 greatly increase T_3. Parameters that increase γ (larger T_L, larger D*, smaller B') will
660 increase T_3.
661 5. Contaminant decay in low K zones can substantially reduce cleanup times when $\lambda_L T_D$ is
662 large. However, decay will have minimal impact on T_{OoM} when $\lambda_L T_D < 0.01$. Given
663 typical values for T_D in LG and BG systems, previously reported decay rates are
664 sufficient to substantially reduce T_3.
665
666 The CM has several important limitations that need to be considered when applying this
667 approach to a specific site.
668 1. The CM was developed based on 1D simulations using REMChlor-MD (Falta et al.,
669 2018) and all results are subject to the limitations of this approach.

2. The regression equations are developed to estimate the time to reach 1, 2 and 3 OoM reductions in the vertically averaged concentrations in monitor wells. When vertical dispersivity is low, concentrations immediately adjoining low K zones will be higher, and longer time periods may be required to reduce concentrations near low K interfaces.
3. The parameter ranges used to generate the LG and BG datasets are intended to cover a broad range of conditions that may occur in unconsolidated sedimentary formations, and so the datasets include some extreme values that may not be representative of typical site conditions. T_{OoM} estimates at the extreme limits of the datasets will be less reliable.
4. In layered aquifers, the LG regression equations are most accurate for $T_D<0.5T_L$. When layer $T_D>2T_L$, T_{OoM} is more accurately estimated using the BG regressions. For T_D between $0.5T_L$ and $2T_L$, behavior is intermediate between LG and BG.
5. In all simulations, the contaminant concentration discharging from the source area was constant for the loading period, T_L, then was reduced to zero. Yang et al. (2016) showed that gradual changes in contaminant source strength over time influence back diffusion rates, with greater diffusive flux for rapidly depleting sources.
6. In this CM, groundwater velocity in low K zones is assumed to be zero. However, under certain conditions, slow advection through low K zones can substantially increase mass transfer between high and low K zones (Li et al. 1994; Guswa and Freyberg, 2000), potentially reducing cleanup times. Research is needed to better understand when slow advection substantially increases mass transfer between high and low K zones.

CRediT authorship contribution statement

Robert C. Borden: Conceptualization, Methodology, Formal Analysis, Writing - original draft, Writing - review & editing, Visualization, Project administration, Funding acquisition. Ki Young Cha: Conceptualization, Methodology, Software, Investigation, Writing - review & editing.

Declaration of competing interest

Robert C. Borden and Ki Young Cha declare no competing interest.

Acknowledgement

This research was conducted with funding from the U.S. Department of Defense Strategic Environmental Research and Development Program (SERDP) Environmental Restoration Program under project ER-2529 entitled "Quantifying Mobile-Immobile Mass Transfer using Direct Push Tools." Thanks to Chuck Newell and Giasheng Liu for the thoughtful review of this manuscript and their helpful insights. This research would not have been possible without the pioneering research by Beth Parker and Steve Chapman on matrix diffusion processes and Ron Falta's development of the semi-analytical model.

710 # References

711

712 Ayral, D. and A.H. Demond, 2014. Estimation of diffusion coefficients for organic solutes of
713 environmental concern in saturated clay-silt mixtures. Clay and Clay Minerals:
714 Geological Origin, Mechanical Properties and Industrial Applications, pp.45-66.

715 Carey, G.R., E.A. McBean, and S. Feenstra, 2016. Estimating tortuosity coefficients based on
716 hydraulic conductivity. Groundwater, 54(4), pp.476-487.

717 Chapman, S.W., and B.L. Parker, 2005. Plume persistence due to aquitard back diffusion
718 following dense nonaqueous phase liquid source removal or isolation. Water Resources
719 Research, 41(12):W12411.

720 Chapman, S.W., B.L. Parker, T.C. Sale, and L.A. Doner, 2012. Testing high resolution
721 numerical models for analysis of contaminant storage and release from low permeability
722 zones. Journal of Contaminant Hydrology, 136: 106-116.

723 Chapman, S.W., and B.L. Parker, 2013. Chapter 5 – Type Site Simulations. In Sale, T., B.L.
724 Parker, C.J. Newell, and J.F. Devlin, 2013. Management of Contaminants Stored in Low
725 Permeability Zones: A State-of-the-Science Review. Strategic Environmental Research
726 and Development Program (SERDP) Project ER-1740, Alexandria, VA 22350-3605.

727 Doner, L.A., 2008. Tools to Resolve Water Quality Benefits of Upgradient Contaminant Flux
728 Reduction (Master Thesis, Colorado State University).

729 Falta, R.W., P.S. Rao, and N. Basu, 2005. Assessing the impacts of partial mass depletion in
730 DNAPL source zones: I. Analytical modeling of source strength functions and plume
731 response. Journal of Contaminant Hydrology, 78(4), 259-280. doi:
732 10.1016/j.jconhyd.2005.05.010

733 Falta, R.W., S.K. Farhat, C.J. Newell, and K. Lynch, 2018. A Practical Approach for Modeling
734 Matrix Diffusion Effects in REMChlor (ER-201426). Environmental Science and
735 Technology Certification Program, Arlington, VA.
736 Farhat, S.K., D.T. Adamson, A.R. Gavaskar, S.A. Lee, R.W. Falta, and C.J. Newell, 2020.
737 Vertical discretization impact in numerical modeling of matrix diffusion in contaminated
738 groundwater. Groundwater Monitoring & Remediation, 40(2): 52-64.
739 Farhat, S.K., C.J. Newell, T.C. Sale, D.S. Dandy, J.J. Wahlberg, M.A. Seyedabbasi, J.M.
740 McDade, and N.T. Mahler. 2012. Matrix diffusion toolkit User's manual. ESTCP Project
741 ER-201126. https://www.serdp-estcp.org/Program-Areas/Environmental-
742 Restoration/Contaminated-Groundwater/Persistent-Contamination/ER-201126/ER-
743 201126.
744 Geosyntec Consultants, 2020. Remedial Measures Annual Report – January 2020, PFC, 3975
745 East Railroad Ave, Cocoa, FL.
746 Grathwohl, P. 1998. Diffusion in Natural Porous Media: Contaminant Transport,
747 Sorption/Desorption and Dissolution Kinetics. Boston, Kluwer Academic Publishers.
748 Grisak, G.E. and J.F. Pickens, 1980. Solute transport through fractured media: 1. The effect of
749 matrix diffusion. Water Resources Research, 16(4): 719-730.
750 Guswa, A.J. and D.L. Freyberg, 2000. Slow advection and diffusion through low permeability
751 inclusions. Journal of contaminant hydrology, 46(3-4): 205-232.
752 Halloran, L.J. and D. Hunkeler, 2020. Controls on the persistence of aqueous-phase groundwater
753 contaminants in the presence of reactive back-diffusion. Science of The Total
754 Environment, 722, p.137749.

Li, L., D.A., Barry, P.J. Cuiligan-Hensley, and K. Bajracharya, 1994. Mass transfer in soils with local stratification of hydraulic conductivity. Water Resources Research, 30(11): 2891-2900.

Liu, C. and W.P. Ball, 2002. Back diffusion of chlorinated solvent contaminants from a natural aquitard to a remediated aquifer under well-controlled field conditions: Predictions and measurements. Groundwater, 40(2): 175-184.

Mackay, D. M., R. D. Wilson, M. J. Brown, W. P. Ball, G. Xia, and D. P. Durfee, 2000. A controlled field evaluation of continuous vs. pulsed pump-and-treat remediation of a VOC-contaminated aquifer: site characterization, experimental setup, and overview of results. Journal of Contaminant Hydrology 41(1-2): 81-131.

Muskus, N. and R.W. Falta, 2018. Semi-analytical method for matrix diffusion in heterogeneous and fractured systems with parent-daughter reactions. Journal of Contaminant Hydrology, 218: 94-109.

Parker, B.L., S.W. Chapman, and M.A. Guilbeault, 2008. Plume persistence caused by back diffusion from thin clay layers in a sand aquifer following TCE source-zone hydraulic isolation. Journal of Contaminant Hydrology, 102(1-2), pp.86-104.

Parker, J.C. and E. Park, 2004. Modeling field-scale dense nonaqueous phase liquid dissolution kinetics in heterogeneous aquifers. Water Resources Research, 40(5). doi: 10.1029/2003WR002807

Sale, T.C., J.A. Zimbron, and D.S. Dandy, 2008. Effects of reduced contaminant loading on downgradient water quality in an idealized two-layer granular porous media. Journal of Contaminant Hydrology 102(1-12): 72-85.

Sall, J., M.L. Stephens, A. Lehman, and S. Loring, 2017. JMP start statistics: a guide to statistics and data analysis using JMP. SAS Institute.

Schaefer, C.E., P. Ho, E. Berns, and C. Werth, 2018. Mechanisms for abiotic dechlorination of trichloroethene by ferrous minerals under oxic and anoxic conditions in natural sediments. Environmental Science & Technology, 52(23), pp.13747-13755.

Tatti, F., M.P. Papini, G. Sappa, M. Raboni, F. Arjmand, and P. Viotti, 2018. Contaminant back-diffusion from low-permeability layers as affected by groundwater velocity: A laboratory investigation by box model and image analysis. Science of The Total Environment, 622, pp.164-171.

Wanner, P., B.L. Parker, S.W. Chapman, R. Aravena, and D. Hunkeler, 2016. Quantification of degradation of chlorinated hydrocarbons in saturated low permeability sediments using compound-specific isotope analysis. Environmental Science & Technology, 50(11), pp.5622-5630.

Wanner, P., B.L. Parker, S.W. Chapman, G. Lima, A. Gilmore, E.E. Mack, and R. Aravena, 2018. Identification of degradation pathways of chlorohydrocarbons in saturated low-permeability sediments using compound-specific isotope analysis. Environmental Science & Technology, 52(13), pp.7296-7306.

Yang, M., M.D. Annable, and J.W. Jawitz, 2015. Back diffusion from thin low permeability zones. Environmental Science & Technology, 49(1), pp.415-422.

Yang, M., M.D. Annable, and J.W. Jawitz, 2016. Solute source depletion control of forward and back diffusion through low-permeability zones. Journal of Contaminant Hydrology, 193, pp.54-62.

799 Zech, A., S. Attinger, V. Cvetkovic, G. Dagan, P. Dietrich, A. Fiori, Y. Rubin, and G. Teutsch,
800 2015. Is unique scaling of aquifer macrodispersivity supported by field data?. Water
801 resources research, 51(9), pp.7662-7679, doi:10.1002/2015WR017220.
802
803

804 **Graphical Abstract**

805

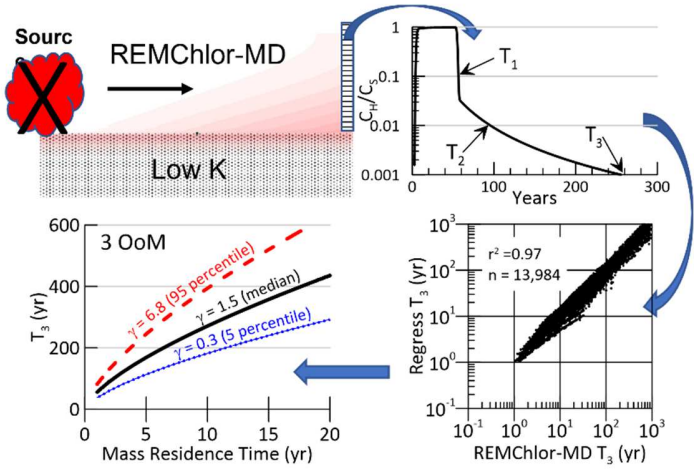

806

807

808

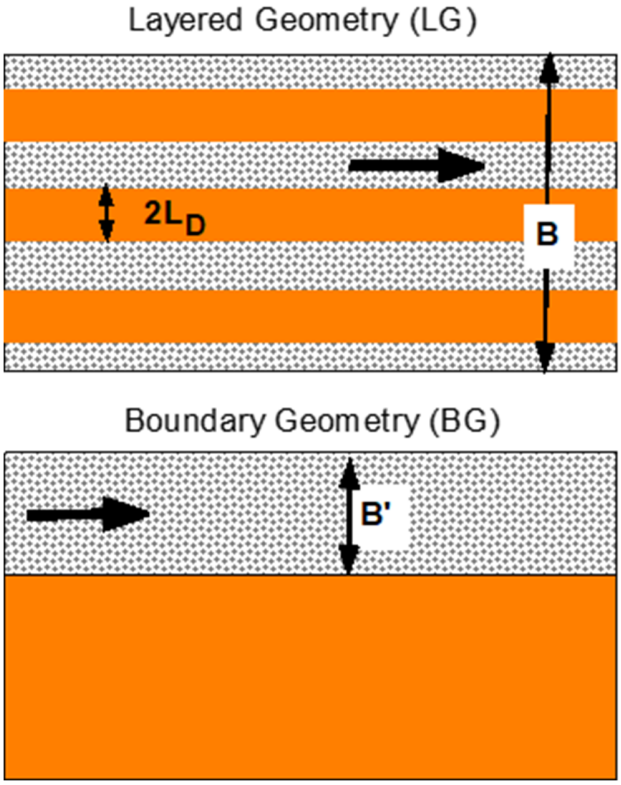

809

810 Figure 1. Aquifer conditions evaluated: a) layer geometry (LG) containing finite thickness low

811 K layers; and b) boundary geometry (BG) with extensive low K boundaries.

812

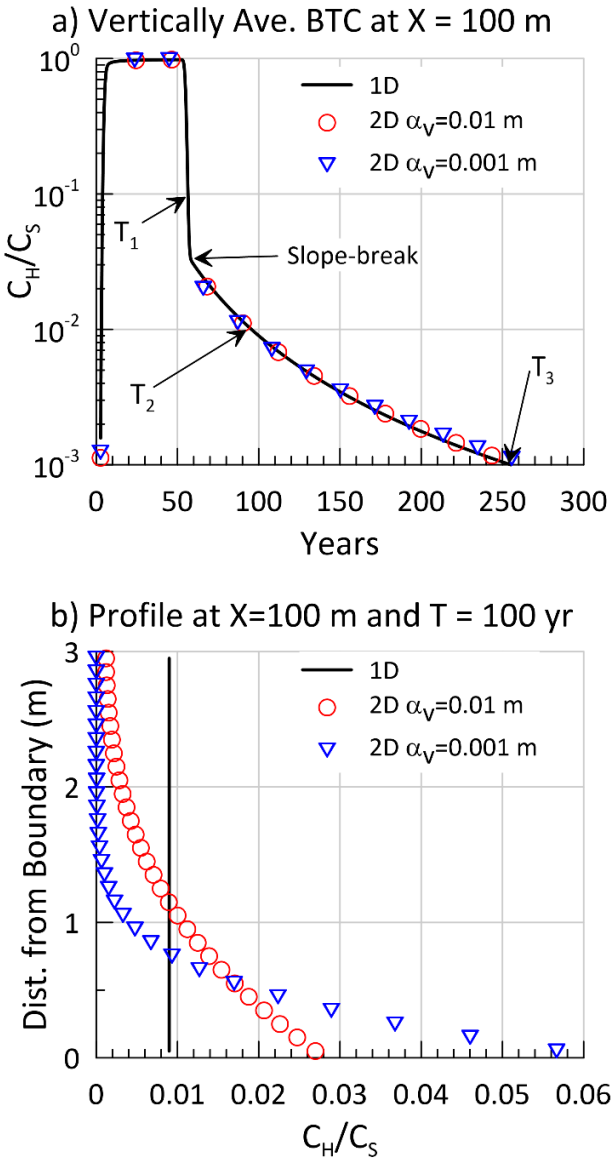

Figure 2. Comparison of 1D and 2D simulation results: a) vertically averaged concentration breakthrough curves (BTC) at X=100 m; and b) vertical concentration profiles at X=100 m and T=100 yr.

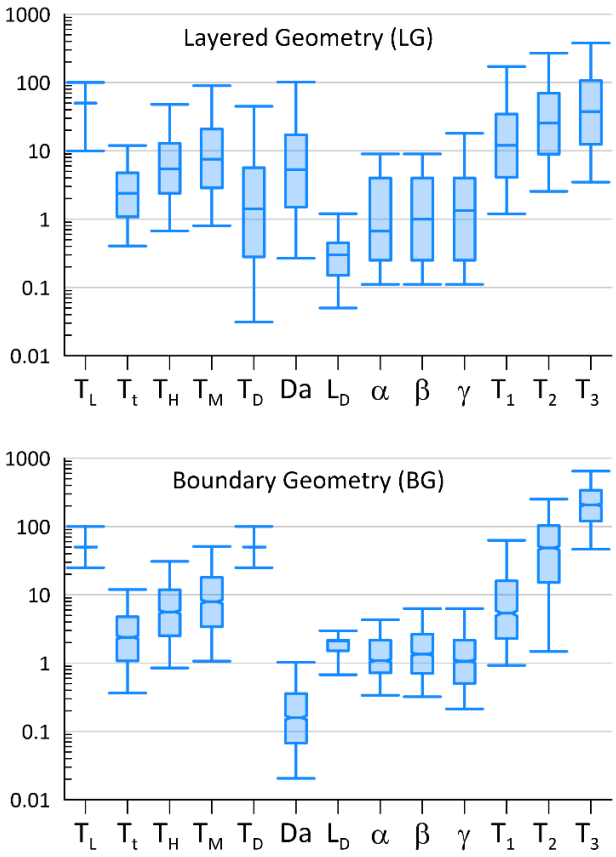

Figure 3. Scaling parameters for layered geometry (LG) and boundary geometry (BG) datasets without decay (λ_L=0). Time in yr, distance in m. Plots show median, 25%/75% box and 5%/95% whiskers.

826

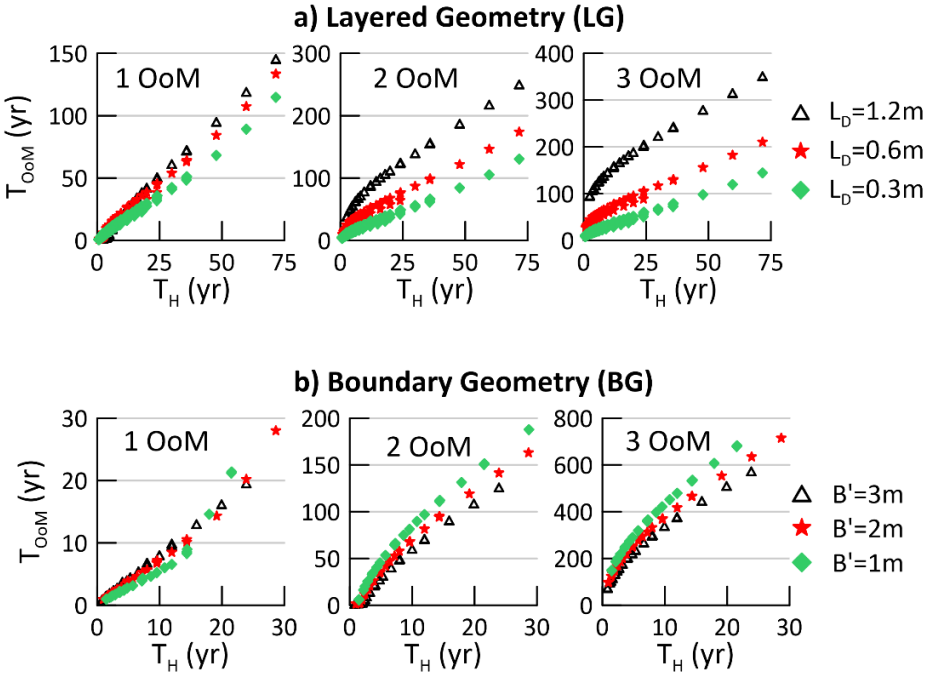

827

828 Figure 4. Impact of varying hydraulic retention time (T_H), diffusion length (L_D), and normalized

829 aquifer thickness (B') on T_{OoM} for 1, 2 and 3 OoM reductions for base case conditions. Note

830 different vertical axes for 1, 2 and 3 OoM.

831

832

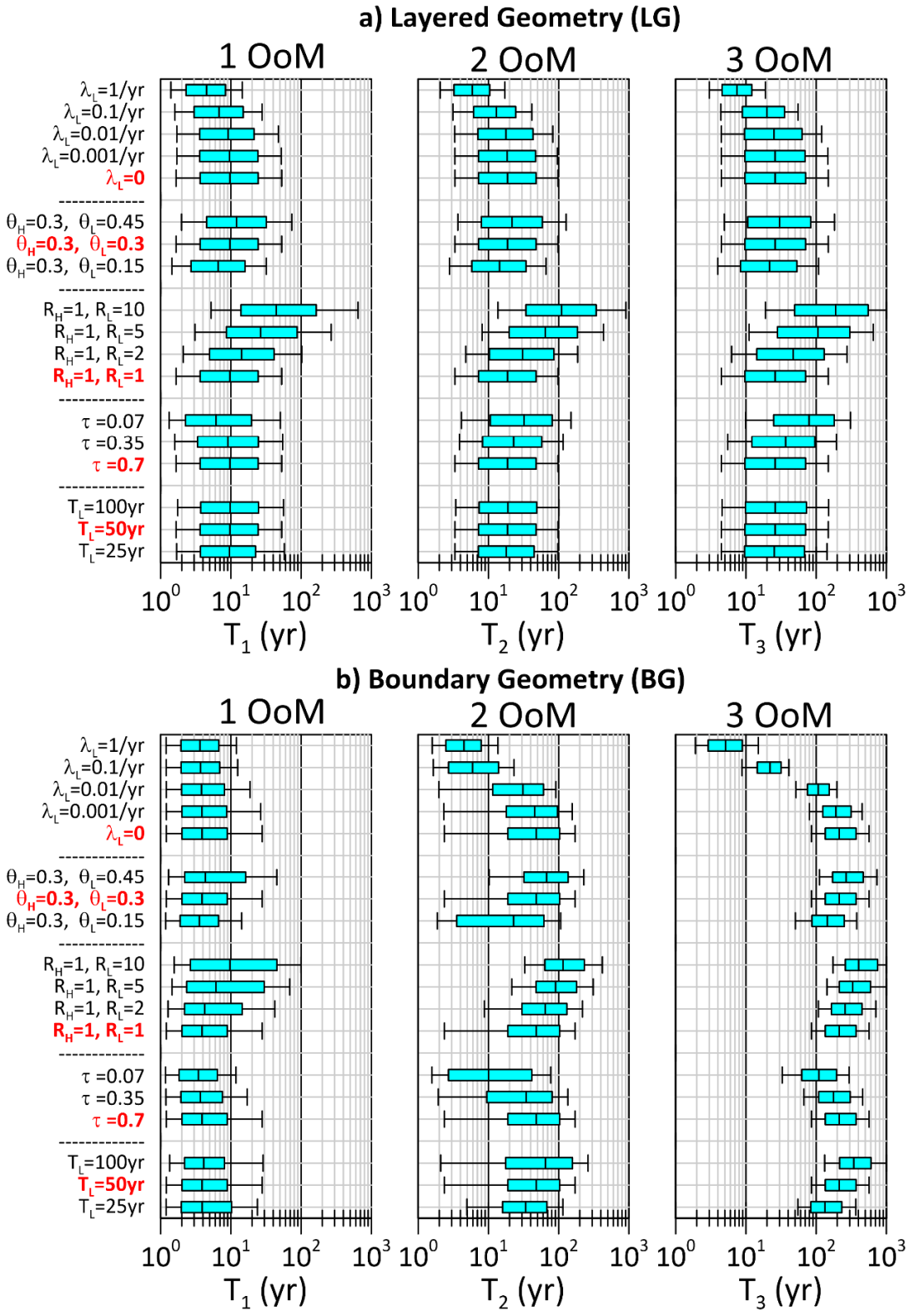

Figure 5. Effect of varying input parameters on distributions of T_1, T_2 and T_3 for LG and BG. Plots show median, 25%/75% box and 5%/95% whiskers. Base case values highlighted in red.

836

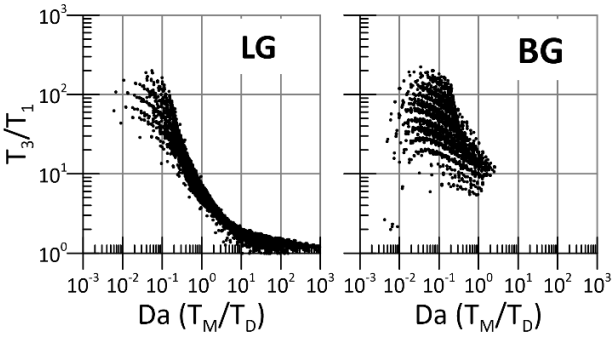

837

838 Figure 6. Ratio of T_3/T_1 with no decay (λ_L =0) versus Damköhler number (Da) for LG and BG.

839

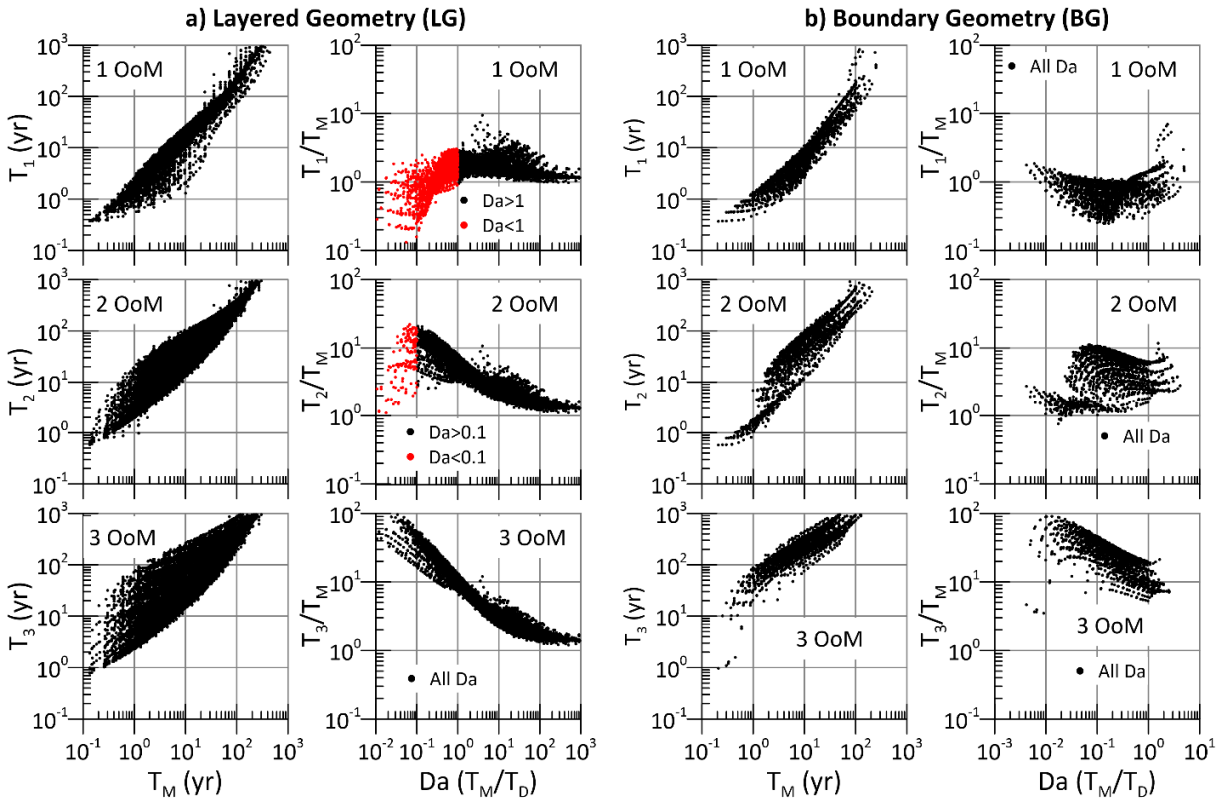

Figure 7. T_{OoM} versus T_M and T_{OoM}/T_M versus Da for layered and boundary geometry.

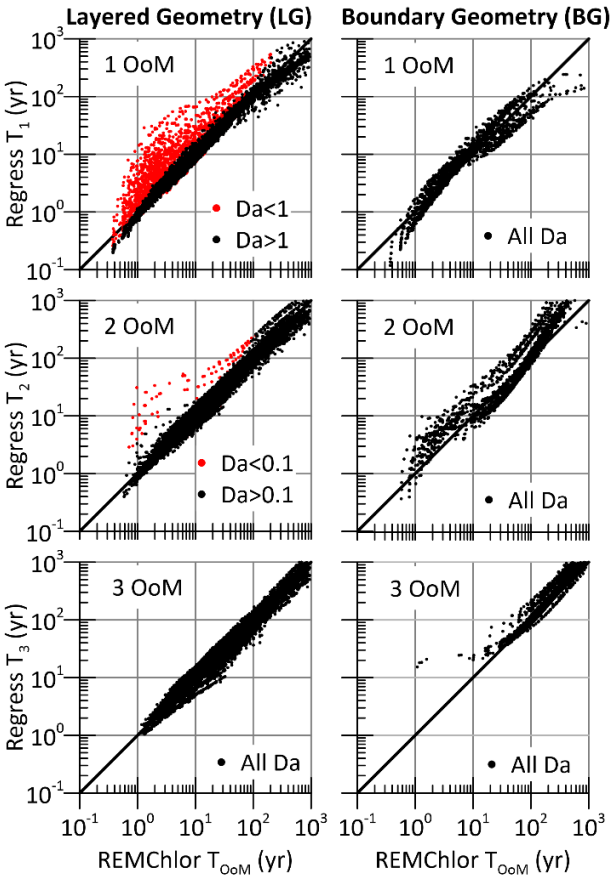

Figure 8. Comparison of 1, 2 and 3 OoM cleanup times calculated with RemChlor-MD and simplified regression equations for layered geometry (LG) and boundary geometry (BG).

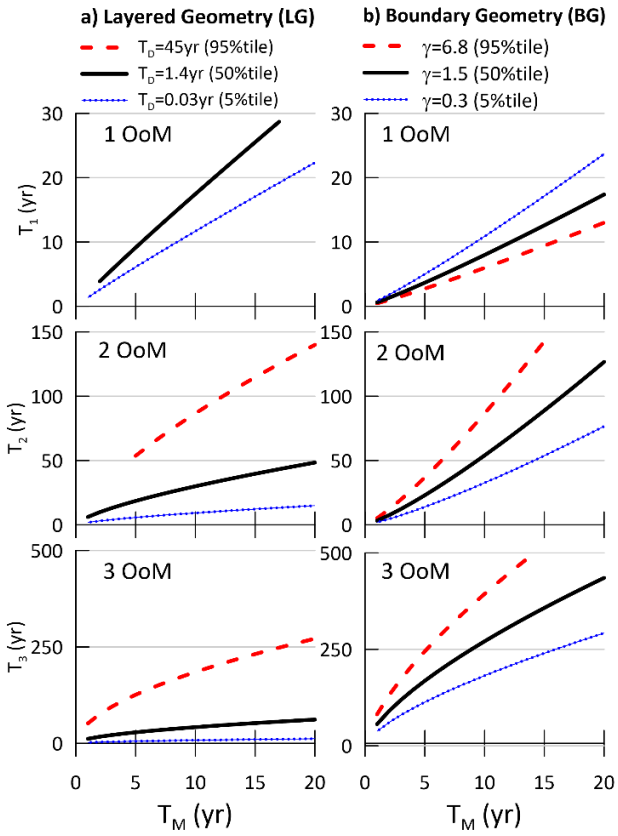

Figure 9. Variation in cleanup time estimated with Eq. 1 for layered geometry and boundary geometry. Values of T_D and γ are 5, 50 and 95 percentile values for the dataset.

858

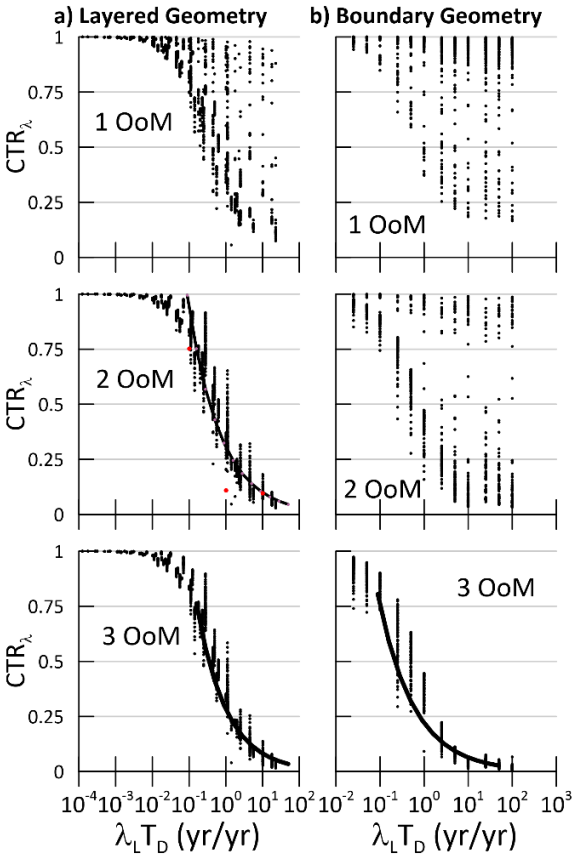

859

860 Figure 10. CTR_λ versus $\lambda_L T_D$ for a) layered geometry; and b) boundary geometry. Coefficients

861 for regressions (solid black line) in Table 4.

862

863

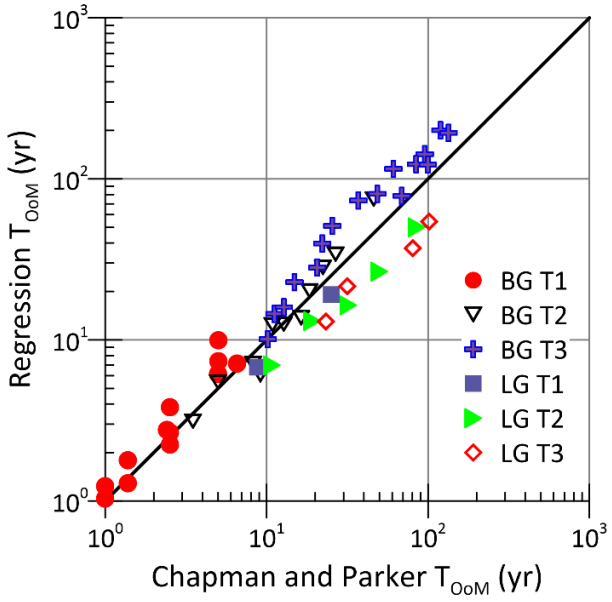

Figure 11. Comparison of cleanup time estimates from regression equations and high-resolution numerical simulations by Chapman and Parker (2013).